*17th World Conference on Earthquake Engineering, 17WCEE*
*Sendai, Japan - September 27th to October 2nd, 2021*

# PERFORMANCE UNDER CYCLIC LOADING OF SQUARE HSS BRACES WITH INTENTIONAL ECCENTRICITY (BIEs)

A. González Ureña[(1)], R. Tremblay[(2)], C.A. Rogers[(3)]

[(1)] *Ph.D. candidate, Department of Civil Engineering, McGill University, andres.gonzalezurena@mcgill.ca*
[(2)] *Professor, Department of Civil, Geological and Mining Engineering, Polytechnique Montréal, robert.tremblay@polymtl.ca*
[(3)] *Professor, Department of Civil Engineering, McGill University, colin.rogers@mcgill.ca*

## *Abstract*

Braces with Intentional Eccentricity (BIEs) are a recently proposed type of lateral bracing system that surmounts several of the shortcomings that Conventional Concentric Braces (CCB) present. As their longitudinal axis is deliberately offset with respect to the line of action of the forces acting on them, BIEs are subject to bending moment in addition to axial forces and, as such, they are naturally less stiff than CCBs. Their stiffness can be adjusted directly by varying the eccentricity. They present a trilinear response to loading in tension, with significant post-yielding stiffness, and a smooth flexural behaviour in compression. Moreover, they are presumed to have longer fracture life under cyclic loading because the onset of local buckling is delayed, due to the strains being more evenly distributed along the bracing member's length owing to the flexural response. The application of BIEs to building design has been investigated by the authors with results from numerical analyses showing that Frames with Intentionally Eccentric Braces (FIEBs) could present an improved seismic performance, in terms of maximum and residual storey drifts, in comparison with Concentrically Braced Frames (CBFs). Also, as the shear strength in each storey can be adjusted to match closely the demand by varying the eccentricity of the bracing members, the overstrength can be better controlled, which results in requiring less overall material when incorporating capacity design concepts for the complete Seismic-Force-Resisting System (SFRS).

In this article, the results of the physical testing under cyclic load of four full-scale ASTM A1085 HSS BIE specimens are presented. The introduction of the eccentricity was achieved by means of two parallel side plates linking the HSS to a knife plate; this configuration was selected for its constructability. The knife plate was detailed to yield in flexure to allow for the unrestrained rotation of the brace ends. The results show that the so constructed BIEs display the expected behaviour and purported benefits of the intentional eccentricity and suggest that the magnitude of the eccentricity plays a significant role in determining their fracture life. Additionally, the results showcased that in lieu of fracture at mid-length after the onset of local buckling, fracture of the tested BIEs could occur at the bracing member's ends under tensile load, which was attributed to excessive localized rotational demand on the HS member.

*Keywords: Braces with Intentional Eccentricity; Steel braced frames; Earthquake-Resistant Design; Physical Testing*

## 1. Introduction

Braces with Intentional Eccentricity, steel braces whose longitudinal axis is offset with respect to the line of action of the forces transmitted through them, have been proposed by Skalomenos et al. [1] as an alternative to Conventional Concentric Braces (CCBs) offering an enhanced performance under earthquake loading. Due to the eccentricity, axial loading in BIEs implies bending; hence, they are inherently more flexible than CCBs. Moreover, under tension BIEs display substantial post-yielding stiffness as yielding progresses gradually through the cross-section, producing a trilinear response unlike CCBs, which display instead an elastic-perfectly plastic behaviour. Under compression, BIEs offer a smooth flexural response, without the marked loss in strength associated with global buckling that is characteristic of CCBs. However, the most advantageous feature of BIEs is that their stiffness and their strength at a given displacement level can be adjusted directly by varying the prescribed eccentricity, thus granting the designer with a significantly enhanced control over the overstrength and the dynamic response of the structure.

In addition to this, it is apparent that the eccentricity grants BIEs a longer fracture life than CCBs under cyclic loading, in terms of allowable displacement or equivalent drift ratio. Owing to the flexural component of the response, longitudinal strains under compression and flexure are more evenly distributed over the bracing member's length, instead of concentrating at mid-length from an early stage, thus delaying the onset of local buckling and subsequent low-cycle fatigue fracture. Modern design provisions, such as those of the CSA S16 Standard [2], impose stringent limits on the local and global slenderness ratios for hollow structural sections (HSSs) used as CCBs for seismic application, with the intent of reducing the probability of fracture by proscribing excessively stocky or non-compact braces. Arguably, the use of BIEs could permit more relaxed limits, enlarging the array of useable HSS brace members.

In studying the application of BIEs to building structures, the authors developed an expression to estimate the fracture life of BIEs for design purposes as a function of their global and local slenderness and eccentricity [3], and proposed a displacement-based procedure for the design of Frames with Intentionally Eccentric Braces (FIEBs) [4, 5]. The numerical simulations performed showed FIEBs display a seismic performance superior to that of Concentrically Braced Frames (CBFs) with CCBs, in terms of maximum and residual drift ratios, while requiring significantly less material. Skalomenos et al. [1] introduced the concept of the BIE and reported on the physical testing of five half-scale BIE specimens based on a single round HSS; their results are consistent with the behaviour described above and showcase the purported advantages of BIEs over CCBs. This article presents a summary of the results of a laboratory test program in which four full scale ASTM A1085 square HSS BIE specimens, along with one reference CCB specimen, were tested under reversed cyclic loading. For a comprehensive report on the general properties of BIEs and their force-deformation response, the reader is suggested to refer to [5].

## 2. Laboratory test program

### 2.1 Specimen selection and design

As mentioned, a presumed benefit of the intentional eccentricity is that it could allow for HSS bracing members that would be considered overly stocky and/or non-compact for use in CBFs, to extend their fracture life to an extent which would make them apt for use in FIEBs. With this hypothesis in consideration, the test specimens were selected with the intent of studying the behaviour of braces complying with or exceeding the limits on the global and local slenderness ratios specified in the CSA S16 Standard. In this standard, the global slenderness is quantified by the effective length to radius of gyration ratio, $KL/r$, which must not be less than 70 for HSS bracing members. For rectangular or square HSSs, local slenderness is associated with the width to thickness ratio of the walls of the cross-section, $b_{el}/t$, and the prescribed limit varies linearly from $330/\sqrt{F_y}$ for braces with $KL/r$ of 100 or lower, to $420/\sqrt{F_y}$ for braces with slenderness ratio of 200, where $F_y$ is the yield strength of the material. The length of the test specimens was established assuming braces used in hypothetical braced bents 6 m wide and 4 m tall, accounting for an estimation of the sizes of the implicated



 

connections, beams, and columns. These bay dimensions were embraced because they represent a typical mid-rise CBF, and because they are compatible with the installed large-scale test frame and especially designed apparatus for brace testing available in the Polytechnique Montréal's Structures Laboratory.

The list of test specimens, their sections, eccentricities, and global and local slenderness ratios are presented in Table 1. For Specimens 1 and 2, an HSS 127×127×7.9 was selected as it produced braces complying with both slenderness limits. Specimen 2 had an eccentricity $e$ of 130 mm (Fig. 1), resulting in an eccentricity to depth, $e/d$, ratio of approximately 1.0. Specimen 1 was designed as a reference CCB intended to provide complementary data for comparison. Specimen 3 employed an HSS 254×254×13, resulting in a global slenderness ratio lower than the prescribed CSA S16 limit but a complying local slenderness; its eccentricity was 200 mm for an $e/d$ ratio close to 0.8. Specimen 5 was identical to Specimen 3, except for having a 50% larger eccentricity at 300 mm. Finally, Specimen 4 had the same eccentricity and global slenderness as Specimen 3, but with an HSS 254×254×10; as such, its local slenderness was deliberately greater than that allowed by CSA S16.

Table 1 – List of brace test specimens

| Specimen | Section | Eccentricity, $e$ (mm) | Eccentricity ratio, $e/d$ | Global slenderness, $KL/r$ | Local slenderness, $b_{el}/t$ | Limit $b_{el}/t$ |
|---|---|---|---|---|---|---|
| 1 | 127×127×7.9 | 0 | 0 | 114.0 | 12.0 | 18.4 |
| 2 | 127×127×7.9 | 130 | 1.02 | 114.0 | 12.0 | 18.4 |
| 3 | 254×254×13 | 200 | 0.79 | 47.5 | 16.0 | 17.8 |
| 4 | 254×254×9.5 | 200 | 0.79 | 46.8 | 22.7 | 17.8 |
| 5 | 254×254×13 | 300 | 1.18 | 47.5 | 16.0 | 17.8 |

The design of the BIE specimens was based on the conceptual arrangement shown in Fig. 1. The *eccentering* assemblies, that is, the components of the BIE whose function is to accommodate the eccentricity while transmitting rigidly the forces between the bracing member and the connections to the frame beam-column joints, are composed of side plates that are connected by flare bevel welds to the corners of the HSS. These side plates are welded to a knife plate for which a clearance, $L_k$, is detailed to create a hinge and achieve an in-plane pin-like behaviour. The knife plate is slotted perpendicularly into a gusset plate to which it is connected by four bolted angles. In a real FIEB, the gusset plate would be welded to the inside of the beam-column joint; in the case of the test specimens, the gusset plates were designed as T-stubs to be inserted and secured inside a set of grips attached to the testing frame to apply the loading, as presented in Fig. 2. This arrangement, also used in the numerical analyses in [4] and [5], was adopted because of its constructability and since it permitted the reuse of the T-stubs, of which only two pairs were fabricated: one for use with Specimens 1 and 2, and another, larger, for Specimens 3, 4, and 5. Given the specimens' orientation in the test frame, flexural deformation was confined to the north-south plane, with compression producing deflection toward the north.

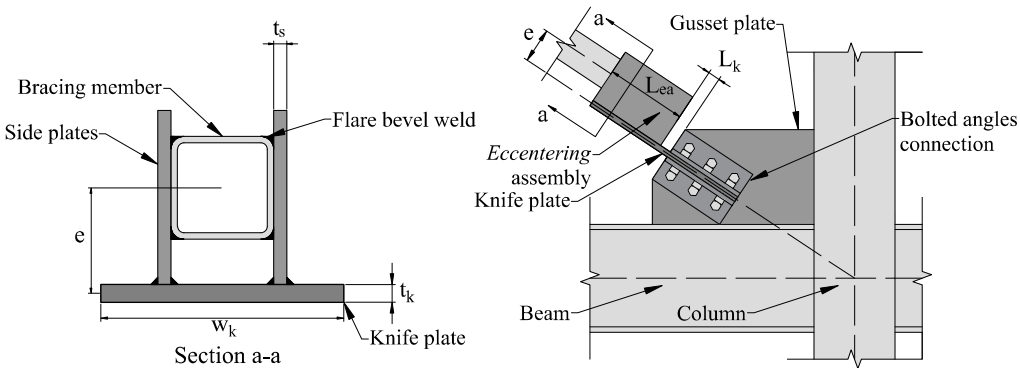


Fig. 1 – Considered BIE-to-frame connection and *eccentering* assembly concept



 

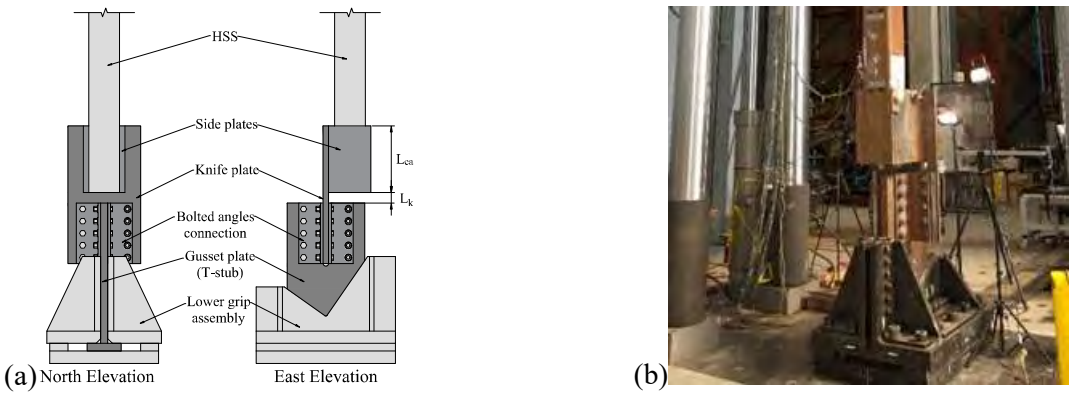


Fig. 2 – Detail of Specimen 5 and T-stub attached to lower grip assembly: drawing (a) and photograph (b)

The detailed dimensions of the five specimens are presented in Table 2. As indicated in Fig. 1, $t_k$, $w_k$, and $L_k$ are the thickness, the width, and the hinge length of the knife plate, whereas $t_s$ and $L_{ea}$ are the thickness and length of the side plates constituting the *eccentering* assembly The dimension $L$ corresponds to the total, or hinge-to-hinge length of the BIE, taken as the distance between the far ends of the *eccentering* assemblies, $d$ and $t$ are the depth and thickness of the HSS cross-section. In Specimen 1, the knife plate was directly slotted into the HSS and cover plates were used to reinforce the connection and prevent a net section fracture at that location. For this specimen, $L_{ea}$ indicates the length over which the HSS and knife plate overlap. All bracing members were ASTM A1085 HSS and all plate components were made with ASTM A572 grade 50 steel. Both materials have specified minimum yield stress $F_y$ of 345 MPa and tensile strength $F_u$ of 450 MPa.

Table 2 – Dimensions of BIE test specimens

| Specimen | $d$ (mm) | $t$ (mm) | $e$ (mm) | $L$ (mm) | $L_{ea}$ (mm) | $w_k$ (mm) | $L_k$ (mm) | $t_s$ (mm) | $t_k$ (mm) |
|---|---|---|---|---|---|---|---|---|---|
| 1 | 127 | 7.94 | 0 | 5470 | 300 | 300 | 44 | N/A | 22 |
| 2 | 127 | 7.94 | 130 | 5470 | 300 | 300 | 44 | 16 | 22 |
| 3 | 254 | 12.7 | 200 | 4640 | 550 | 600 | 88 | 32 | 32 |
| 4 | 254 | 9.53 | 200 | 4640 | 550 | 600 | 88 | 32 | 32 |
| 5 | 254 | 12.7 | 300 | 4640 | 550 | 600 | 88 | 32 | 32 |

## 2.2 Loading Protocol

The specimens were subjected to a series of displacement cycles, tension first then compression, as presented in Fig. 3. The amplitude of the applied displacement was defined based on the equivalent drift ratio (EDR) of the 6 m by 4 m braced bent assumed in the specimens' design. Thus, a displacement amplitude of ± 33.3 mm corresponded to a drift ratio of ± 1.0%. For the five specimens, the loading protocol started with two series of 6 cycles with amplitudes of 0.1% and 0.25% EDR, respectively, followed by 2 cycles with 0.5% EDR amplitude and 2 cycles with 0.75% EDR amplitude. After the 0.75% EDR cycles, the protocol included two cycles with 0.1% EDR amplitude, but centred on + 0.1% EDR. These cycles were included to determine the residual stiffness of the braces after sustaining a displacement demand from a seismic event of moderate intensity. Following these low amplitude cycles, the protocol used with Specimens 1 and 2 comprised pairs of cycles with amplitudes of 1.0, 1.5, 2.0, 2.5, 3.0, and 4.0% EDR. For Specimens3, 4, and 5, the protocol was similar but with constant 0.25% EDR amplitude increments at every other cycle. In the tests, the displacements were controlled by the average reading of a pair of string potentiometers that measured the overall elongation of the specimens, including the displacement of their connections to the T-stubs. The displacement rate was kept fixed at 0.33 mm/s to avoid any dynamic or strain rate effects. All tests were carried out up to complete fracture of the specimens.



 

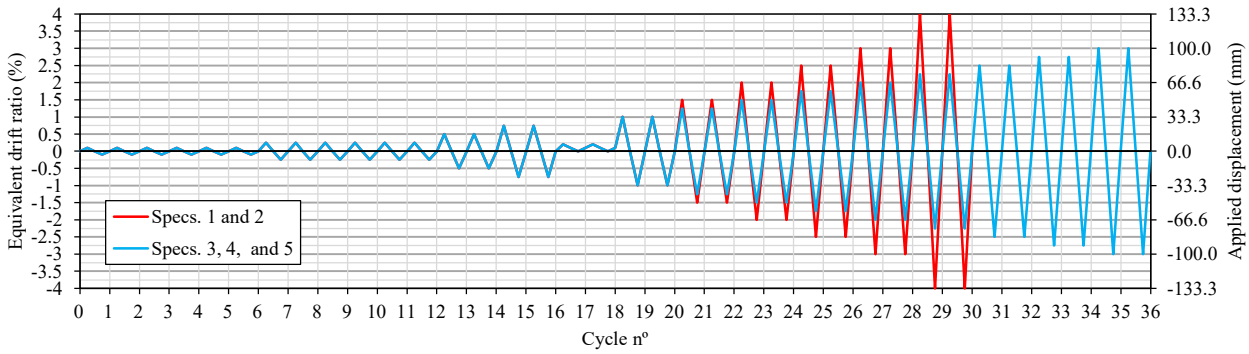


Fig. 3 – Loading protocol

## 2.3 Results

The recorded axial force vs. equivalent drift ratio hysteresis plots for the five specimens are presented in Fig. 4. Table 3 contains a summary of the most relevant test results and observations. To allow for a more direct comparison of the specimens' behaviour, idealised backbone curves were constructed and used to obtain experimental values of the axial load and displacement at the first yield point, $T_y$ and $\delta_y$, the compressive resistance, $C'$, and the initial and secondary stiffnesses, $K_i$ and $K_s$. These curves were constructed as per the theoretical model described in [4], assuming a bilinear response in tension, with positive secondary stiffness, and an elastic-perfectly plastic behaviour in compression. The values of $T_y$ and $C'$ were calibrated such that the area under the backbone was equal to the area under the exterior envelope of the plots. However, in contrast with the theoretical model, the last recorded peak in tension was taken as the point defining the end of the inelastic segment in tension, instead of the theoretical point corresponding with the complete yielding of the bracing member's cross-section, $T_u$. For CCB Specimen 1, the backbone curve in compression is not presented as its corresponding behaviour differs substantially from the model proposed for BIEs.

Specimen 1 presented the response expected for a CCB, with a marked maximum in compression and subsequent strength degradation associated with global buckling, and a clear contrast in tension between the elastic and post-yielding stages. As reported in Table 4, its post-yielding stiffness is negligible compared to the elastic stiffness. Local buckling was noted during the first 3% EDR cycle in compression, and the brace fractured at mid-length before attaining the peak in tension of the second 4% EDR cycle – this type of failure is reported as failure mode 'A' in Table 4. This relatively long fracture life is consistent with that expected of a slender brace with a compact cross-section. Due to an accidental misalignment of the bolt holes in the fabrication of the T-stubs used with Specimens 1 and 2, it was necessary to enlarge the bolt holes of the angles to allow the installation of the specimen. This resulted in slipping of the connections with a magnitude of ± 22 mm occurring at a load of approximately ± 250 kN, as can be observed in Fig. 4 (a). For this reason, the intended displacement history could not be effectively applied to the brace specimen. This affected the measured stiffness, but did not alter significantly the overall response of the specimen and the measured peak force values.

Specimen 2 presented a behaviour markedly distinct from that of CCBs, with a significant post-yielding stiffness in tension, approximately 26% of the elastic stiffness. In compression, it exhibited a stable flexure response with no signs of global nor local buckling. Before reaching the first 2.0% EDR peak, fracture of the HSS initiated on the South face, at the end of the welds connecting HSS to the top *eccentering* assembly, as shown in Fig. 5. Loading was continued and complete HSS fracture occurred before reaching the first 2.5% EDR peak in tension. This failure mode, referred to as type 'B' in Table 4, is attributed to the large strains that concentrated in the HSS as a consequence of the large rotation demands derived from the BIE's kinematic response, as further expanded below. Had the HSS in Specimen 2 the same material properties as those of Specimen 1, the maximum load in tension was of approximately 58% of the theoretical tension strength of its cross-section. Although the holes of the angles of Specimen 2 also had to be enlarged, the specimen response was not significantly affected by the slippage at the connections.



 

Specimens 3, 4 and 5 also displayed the behaviour expected for BIEs, with substantial post-yielding stiffness and a smooth response in compression, prior to the onset of local buckling. Nonetheless, their failure mode consisted of fracture at mid-length of the HSS after occurrence of local buckling in that region. Initiation of the low-cycle fatigue fracture of Specimen 5 is shown in Fig. 6. The comparison of the results of Specimens 5 and 3 show that the additional eccentricity increased significantly the fracture life of the brace, delaying the onset of local buckling from the first 1.75% EDR cycle to the second 2.25% EDR cycle, at the expense of equivalently reduced stiffness and strength. Specimen 4 sustained the earliest local buckling and fracture among all specimens, as was expected in view of its largest local slenderness. For that specimen, local buckling occurred during the first 1.25% EDR cycle, which would not be acceptable for FIEBs such as those discussed in [4] and [5], for which the minimum target design drift ratio is 1.5%. Comparing the results from Specimens 3 and 4, it can be noted that the values of $K_i$, $T_y$, and $C'$ of the latter are approximately 20% lower than those of Specimen 3, suggesting a correlation with the HSS cross-section area, as the ratio of the nominal areas of both specimens is approximately 80%. The reported secondary stiffness, however, was nearly the same for both specimens.

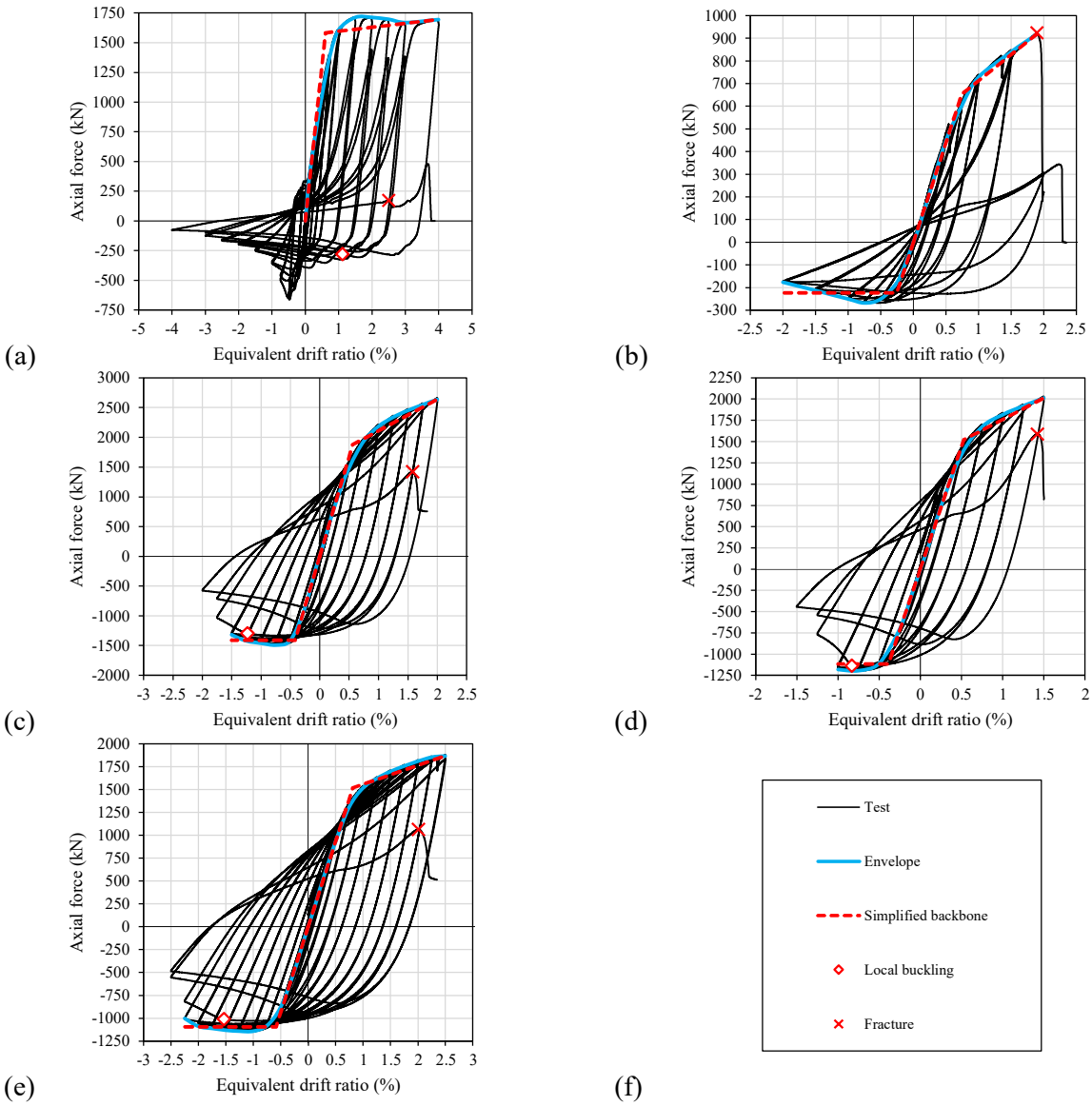


Fig. 4 – Axial force vs. equivalent drift ratio, envelope, and simplified backbone curves: Specimen 1 (a), Specimen 2 (b), Specimen 3 (c), Specimen4 (d), Specimen 5 (e), and legend (f)



 

Table 3 – Summary of BIE test results

| Spec. | $T_{max}$ (kN) | $C_{max}$ (kN) | Failure mode | Onset of local buckling (EDR cycle) | Fracture (EDR cycle) | $T_y$ (kN) | $C'$ (kN) | $\delta_y$ (mm) | $K_i$ (kN/mm) | $K_s$ (kN/mm) | $\frac{K_s}{K_i}$ |
|---|---|---|---|---|---|---|---|---|---|---|---|
| 1 | 1718 | -691 | A | 1st 3% | 2nd 4% | 1583.7 | N/A | 20.1 | 78.9 | 0.99 | 0.01 |
| 2 | 924 | -267 | B | N/A | 1st 2% | 653.0 | -223.4 | 24.7 | 26.4 | 6.91 | 0.26 |
| 3 | 2664 | -1491 | A | 1st 1.75% | 2nd 2% | 1877.1 | -1412.5 | 18.6 | 100.9 | 15.8 | 0.16 |
| 4 | 2032 | -1192 | A | 1st 1.25% | 2nd 1.5% | 1521.1 | -1117.9 | 17.5 | 86.7 | 15.2 | 0.17 |
| 5 | 1877 | -1146 | A | 2nd 2.25% | 1st 2.75% | 1518.3 | -1093.5 | 27.1 | 56.1 | 6.18 | 0.11 |

Fig. 5 – Fracture in HSS of Specimen 2 (first 2.0% EDR cycle)

Fig. 6 – Low-cycle fatigue fracture in HSS of Specimen 5 (first 2.75% EDR cycle)

In [3], the authors proposed an expression, intended for use in design, to predict the maximum drift ratio, $\theta_{md}$, that BIEs can safely withstand under cyclic loading prior to the onset of local buckling at their mid length. This expression, given by Eq. (1), was developed from the results of a parametric finite element analysis study and relates $\theta_{md}$ with the eccentricity to HSS depth ratio, $e_0 = e/d$, and the combined slenderness ratio, $\lambda_0 = (KL/r)/(b_{el}t)$. The experimental $\theta_{md}$ values, taken as the EDR of the cycle with largest amplitude that the specimens could withstand before occurrence of local buckling, are provided in Table 4, along with those calculated with Eq. (1). As shown, Specimens 1, 3, 4, and 5 could withstand cycles with EDRs significantly larger than those predicted by Eq. (1), which suggests that the equation may be overly conservative for ASTM 1085 HSSs. The material properties considered in the development of Eq. (1) were based on coupon data from the flat walls of CSA G40.20-21 350W Class C HSSs [6], which may explain the differences.

$$\theta_{md} = -0.4312 + 0.1943\lambda_0 + 0.6704e_0 - 0.001319\lambda_0^2 - 0.01833\lambda_0 e_0 + 0.241e_0^2 \quad (1)$$

Table 4 – Experimental and predicted values of $\theta_{md}$

| | Specimen 1 | Specimen 2 | Specimen 3 | Specimen 4 | Specimen 5 |
|---|---|---|---|---|---|
| $\theta_{md}$, experimental (EDR) | 2.5% | >2.0% | 1.5% | 1.0% | 2.0% |
| $\theta_{md}$, Eq. (1) (EDR) | 1.30% | 2.06% | 0.77% | 0.61% | 1.2% |

As described above, the loading protocol included two offset low-amplitude cycles between the 0.75% and 1.0% EDR cycles to estimate the residual stiffness that BIEs would display after being subjected to moderate seismic displacement demands. That residual stiffness was obtained from a linear regression of the load-displacement response of the specimen when loaded in tension in each of the two offset cycles. Measurement of initial and residual axial stiffnesses is illustrated in Fig. 7 for Specimens 1 and 2. The ratios between the residual stiffness in the offset cycles and the initial stiffness are reported in Table 5 for all specimens. The comparison between BIE Specimen 2 and CCB Specimen 1 having the same cross-section,



 

reveals that the former was able to maintain a significantly larger portion of its initial stiffness after withstanding the partial loading history. For Specimens 3, 4 and 5, the initial stiffness was maintained virtually unaffected during the offset cycles. Considering their lower level of damage, FIEBs are expected to offer a better performance in comparison with CBFs in the scenario of aftershocks following a seismic event of moderate intensity.

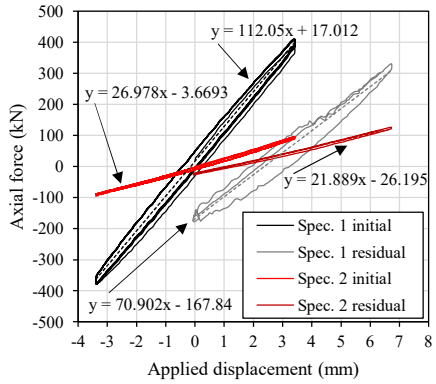


Fig. 7 – Initial stiffness and stiffness during offset cycles for Specimens 1 and 2

Table 5 – Residual stiffness after 0.75% EDR cycles

| Specimen | Post 0.75% stiffness with respect to initial |
|---|---|
| 1 | 63% |
| 2 | 81% |
| 3 | 100% |
| 4 | 99% |
| 5 | 100% |

As opposed to a CCB for which bending only occurs after the brace compressive resistance is exceeded, eccentric loading in a BIE induces bending of the member in both directions about its hinged end connections when subjected to both tension and compression. Kinematically, for a BIE under tension, the rotation at the hinged connections must be compensated by flexure in the bracing member, which would generally lead to the formation of plastic hinges at the HSS ends, in the vicinity of the *eccentering* assemblies. The concentration of rotation at the ends of BIEs under tension is evident in Fig. 8, in which the state of global deformation of Specimen 5 near the peak in tension of the first 2.5% EDR cycle is shown. The rotation history of the bottom *eccentering* assembly of the four BIE specimens is shown in Fig. 9, as recorded by inclinometers mounted on these assemblies. Rotations at the ends of Specimen 1 are also plotted for comparison. These rotations are equal to those sustained by the knife plate over the $L_k$ clear length and, thereby, correspond to the rotations that developed in the plastic hinges at the HSS end, as explained in [5]. In Fig. 9, end rotation in Specimen 1 was only observed after global buckling of the brace, and this rotation occurred in only one direction. Conversely, the ends of the BIEs sustained nearly symmetrical rotations in both directions over the entire duration of the loading history. The rotations that developed in Specimen 2 are considerably higher than those measured in Specimens 3, 4, and 5. Those higher rotations induced the larger strain demands in the HSS south face that led to the premature failure observed for that specimen (Fig. 5).

Fig. 8 – Global deformation of Specimen 5 at the first 2.5% EDR peak in tension



 

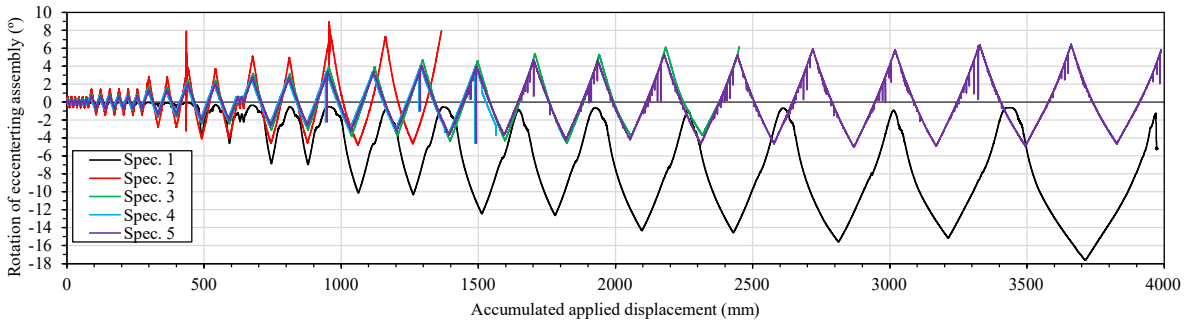


Fig. 9 – Rotation history of bottom *eccentering* assembly (brace end for Specimen 1)

The kinematic response of BIEs also implies that their end connections, detailed with a knife plate clear distance intended to allow for unrestrained rotation, are subjected to rotations demands that are substantially different from the ones in CCBs. Part of the longitudinal strain histories recorded by strain gauges placed at the centre of the south face of the knife plate clear length in Specimens 1 and 2 are provided in Fig. 10. While the south face of the knife plate in Specimen 1 experienced only tension due to bending after brace buckling, the knife plate in Specimen 2 sustained reversed cycles of bending in both directions. Although the adequacy of this type of connection has been demonstrated for use in CBFs, further investigation is needed to verify if the detail can provide a satisfactory performance under the more severe rotational demand imposed by FIEBs, as premature failure at the end connections can compromise the ductility and inelastic deformation capacity of BIEs.

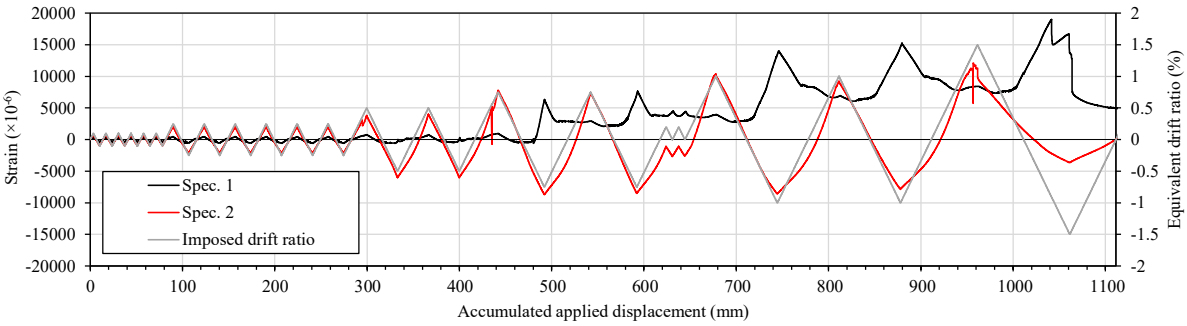


Fig. 10 – Measured strain history in south face of knife plate clearance of Specimens1 and 2

The delay in the onset of local buckling in BIEs with respect to CCBs has been attributed to a strain demand being more evenly distributed along the length of the HSS due to the brace flexural response [1]. To verify the validity of this hypothesis, the strain distribution along the south face of the specimens was studied at the peaks in compression. The distribution of the longitudinal strain gauges along the specimens is shown in Fig 11. The average strains measured by the gauges of groups 2 to 6 on the south face of the specimens are shown in Fig. 12. Strains measured in Specimens 1 and 2 in the first 0.75% EDR cycle are presented in Fig. 12 (a), whereas strains measured in Specimens 3 and 5 in the first 0.5%EDR cycle are shown in Fig. 12 (b). In Specimen 1, strains concentrated predominantly at mid-length of the member. In Specimen 2, strain demands were more balanced between the centre and the quarter length points; however, significant residual strains in tension were measured at the ends of the bracing member in that Specimen. Specimen 5 had a larger eccentricity compared to Specimen 3, which resulted in lower overall strain demands for a given displacement level, as well as a strain more evenly spread along the brace length.

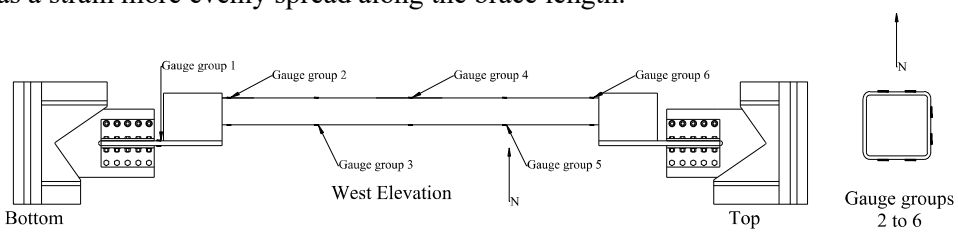


Fig. 11 – Typical strain gauge distribution along brace length and across HSS (Specimen 5 shown)



 

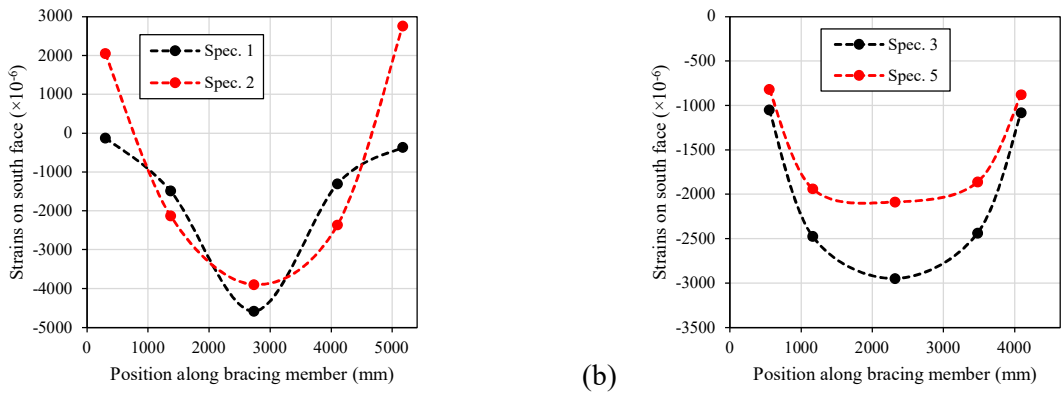


(a) (b)

Fig. 12 – Average measured strains along of the bracing member's south face: Specimens 1 and 2 at the first 0.75% EDR peak in compression (a); Specimens 3 and 5 at the first 0.5% EDR peak in compression(b) (dotted lines are automatically generated trendlines)

In general, strain demands in BIEs were higher under tensile loading than under compressive loading, particularly in the regions adjacent to the *eccentering* assemblies, as the rotational demands were the highest at these locations. The strains measured in the south face of Specimen 2 during the first peaks in compression (a) and in tension (b) of the cycles for each EDR amplitude increment are presented in Fig. 13. In the figure, the square symbols represent data reconstructed or approximated using finite element models, as the data acquisition system during the test was programmed to measure strains up to $\pm 16000\times10^{-6}$. Assuming a yield strain of $\pm 2000\times10^{-6}$, the south face of the bracing member yielded as early as during the first 0.5% EDR cycle. Subsequently, strains at that location surged rapidly as the displacement amplitude increased and, by the 1% EDR cycle, they exceeded ten times the yielding strain. Little of this strain buildup was relieved when the brace was subjected to compression, as can be inferred from Fig. 13 (b), indicating progressive damage to the HSS that ultimately resulted in the tensile fracture failure mode described above (Fig. 5).

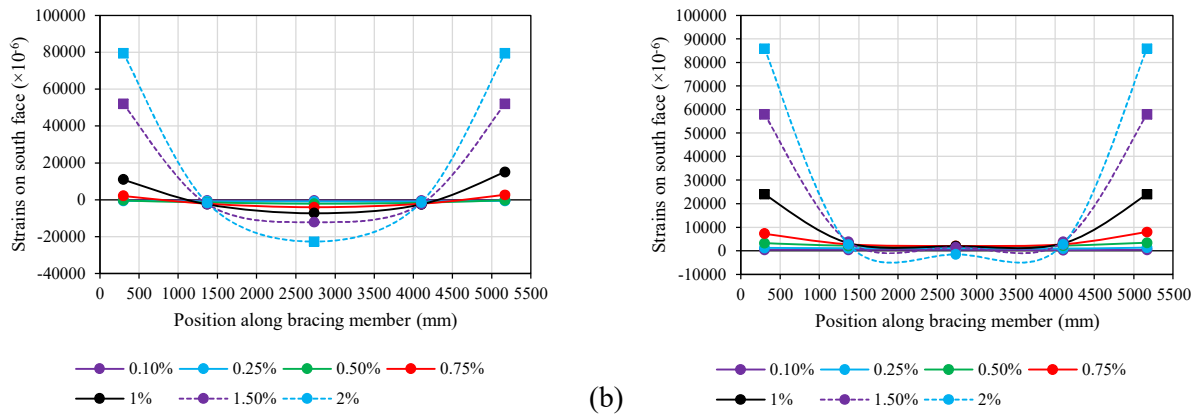


(a) (b)

Fig. 13 – Average measured strain history along south face of Specimen 2: peaks in compression (a), peaks in tension (b) (square symbols indicate data estimated from FE models)

The energy dissipated by the specimens during the first cycle of each EDR increment is presented in Fig. 14 as a function of the EDR amplitude. Comparing the curves obtained for Specimens 3 and 5, the larger eccentricity in Specimen 5 increased the level of displacement at which the BIE attained its maximum energy dissipation capacity, although the magnitude of the maximum energy dissipated during a cycle did not vary significantly. This observation does not apply for Specimens 1 and 2 due to the shorter fracture life of the latter. In general, for BIEs where tensile fracture at the bracing member's ends does not occur, it is expected that increments in the eccentricity lengthen the brace fracture life and increase the total energy dissipated before failure.

In [4] and [5], the use of the equivalent damping ratio is proposed to estimate the net damping capacity of BIEs at a given displacement level that is used to adjust the design displacement spectrum. The model



 

developed in [7] for the prediction of the equivalent damping ratio of CCBs as a function of the ductility demand was considered adequate to be used with BIEs as well, as preliminary numerical results showed that the magnitude of the eccentricity did not significantly affect this variable. The equivalent damping ratio vs. ductility demand curves for the five specimens are presented in Fig. 15. The ductility was calculated by dividing the amplitude of each cycle by the $\delta_y$ values given in Table 2. The results for Specimens 3, 4 and 5 confirm that neither the eccentricity nor local slenderness affected greatly the maximum equivalent damping ratio or the ductility at which it occurred, which supports the appropriateness of the adopted model. For Specimen 1, the curve does not match as well the model as the effective ductility demand on the bracing member could not be properly determined given the significant slippage at the connections.

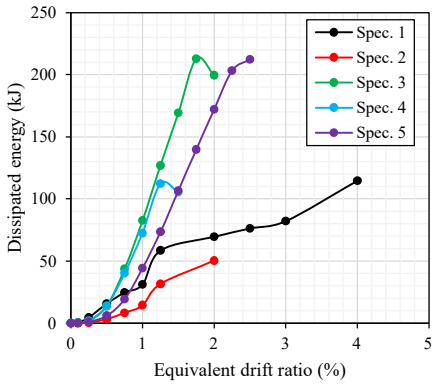


Fig. 14 – Dissipated energy during the first cycle of each EDR increment

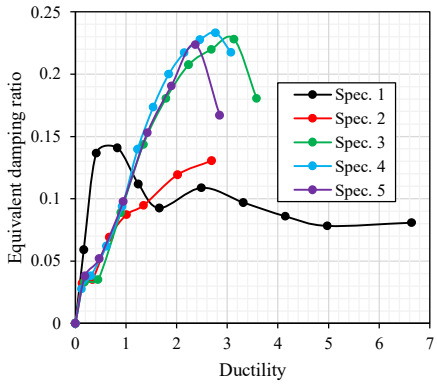


Fig. 15 – Equivalent damping ratio as function of the ductility demand

## 4. Conclusions

A test program was conducted to study the performance under cyclic loading of full-scale BIEs fabricated with square ASTM 1085 HSS members. In the specimens, the eccentricity was introduced by means of side plates welded to the HSS corners that were connected to a knife plate detailed with a clear hinge length to provide unrestrained rotation capacity. The intent was to verify whether the behaviour described in [1] would be reproduced by such braces and explore whether HSS braces not complying with the CSA S16-14 limits on local and global slenderness ratios would display an acceptable cyclic inelastic response with the introduction of an intentional eccentricity.

The results show that, overall, the tested BIE specimens displayed the expected behaviour, including substantial post-yielding stiffness in tension and a stable flexural response in compression prior to the onset of local buckling. Moreover, the tests showed that increasing the magnitude of the eccentricity can delay the onset of local buckling and, thereby, enhance the brace deformation capacity under cyclic loading. This beneficial effect of the eccentricity was further verified by a more even distribution of axial strains in compression along the length of the HSS member. The hysteretic properties of BIEs are expected to reduce the likelihood of a building ratcheting in one direction during an earthquake, in contrast with CBFs that display limited lateral stiffness once the tension brace has yielded and the compression brace has buckled. In addition to this, the test results indicate that BIEs can retain a larger portion of their initial stiffness than CBBs after being subjected to moderate displacement demands. This represents a considerable advantage for FIEBs with respect to CBFs, as the expected damage after a moderate earthquake would be less, warranting an improved response in case of subsequent seismic demands. The results also verified that the equivalent damping ratio of HSS braces is not affected by the magnitude of the eccentricity or the local slenderness of the cross-section. As such, the model developed for CCBs by Wijesundara et al [6] remains an acceptable resource to be employed in displacement-based earthquake-resistant design of FIEBs.

Given the requirement for the connections to accommodate rotation in both directions, the test program raised concerns on whether knife plates or gusset plates detailed with a clear hinge length, widely used with CCBs, would perform equally well for BIEs. While the performance of the knife plate detail used in the tests



 

was satisfactory, the suitability of this type of connection for BIEs designed for significantly larger displacements demands must be investigated.

Finally, the test program showed that fracture under tensile load of the HSS members near the ends is a possible failure mode for BIEs, in addition to fracture at mid-length after the onset of local buckling. Which failure mode governs for a particular BIE is suspected to depend on a combination of geometric factors, including the magnitude of the eccentricity and the relative length of the *eccentering* assemblies and the BIE, as the rotational demand at the brace ends depends on these factors, and on the local slenderness of the HSS cross-section which influences local buckling response. However, the intrinsic non-linearity of the BIE response, both at the geometric and at the material levels, complicates the formulation of a simple relation that would reliably predict the deformation capacity of the bracing member subjected to cyclic inelastic displacement. Furthermore, test data on the rotation capacity of HSSs subjected to axial tension is scarce. Supplementary physical testing of HSS and BIE specimens, along with numerical analyses using advanced finite element models, are required to shed further light on how to predict and thus prevent this failure mode.

## 5. Acknowledgements

The authors would like to thank Atlas Tube and Constructions Proco for donating the required material and fabrication of the test specimens, the staff of the Structures Laboratory at Polytechnique Montréal for their kind collaboration, and DPHV Structural Consultants and ADF Group for their generous technical and financial support, as well as the Natural Sciences and Engineering Council of Canada (NSERC), the Fonds de Recherche du Québec – Nature et Technologies (FRQNT), and the Centre d'Études Interuniversitaire des Structures sous Charges Extrêmes (CEISCE). The authors also express their appreciation to the undergraduate and graduate research assistants from Polytechnique Montréal and McGill University who participated in the test program. Finally, the first author acknowledges the Universidad de Costa Rica for financing the undertaking of his doctoral studies.

## 6. References

[1] Skalomenos K, Inamasu H, Shimada H, Nakashima M (2017): Development of a steel brace with intentional eccentricity and experimental validation. *ASCE Journal of Structural Engineering*, DOI: 10.1061/(ASCE)ST.1943-541X.0001809

[2] CSA (2014): *CSA S16-14: Design of steel structures*. Canadian Standards Association, Toronto, Canada

[3] González Ureña A, Tremblay R, Rogers CA (2020): Numerical investigation of the seismic response of square HSS braces with intentional eccentricity. *17th World Conference on Earthquake Engineering*, Sendai, Japan

[4] González Ureña A, Tremblay R, Rogers CA (2020): Design and performance of frames with intentionally eccentric braces. *17th World Conference on Earthquake Engineering*, Sendai, Japan

[5] González Ureña A, Tremblay R, Rogers CA (2021): Earthquake-resistant design of steel frames with intentionally eccentric braces. *Journal of Constructional Steel Research*, **178**, DOI: 10.1061/J.JCSR.2020.106483

[6] Moreau R (2014): Evaluation of the "Modified-Hidden-Gap" connection for square HSS Brace Members. Master`s thesis, McGill University, Montréal, Canada

[7] Wijesundara K, Nascimbene R, Sulivan T (2011): Equivalent viscous damping for steel concentrically braced frame structures. *Bull. Earthquake Eng.* **9**, 1535-1558



 